



## Water Desalination Graphene Oxide/Ca Ro Membranes Manufactured From Date Palm Fibers' Microcrystalline Cellulose



CrossMark

Tamer I. M. Ragab,<sup>a,\*</sup> Amira A. Fouda,<sup>b</sup> Mohamed M. Azab,<sup>c</sup> Ashraf.A.F. Wasfy,<sup>d</sup> Tarek S. Jamil<sup>e</sup>

<sup>a</sup>Chemistry of Natural and Microbial Products Department, National Research Center, Dokki 12622, Cairo, Egypt

<sup>b</sup>The Holding Company for Drinking Water, Menufia, Egypt

<sup>c</sup>Chemistry Department, Faculty of Science, Benha University, Benha 13518, Egypt

<sup>d</sup>Chemistry Department, Faculty of Science, Benha University, Benha 13518, Egypt

<sup>e</sup>Water Pollution control Department, National Research Center, Dokki 12622, Cairo, Egypt

### Abstract

Egypt produces tons of date palm fibers every year. Fibers of *Phoenix dactylifera* were chemically pulped in here by alkali hydrolysis into hemicellulose, wax, lignin etc... Fractions produced were chemically characterized via spectroscopic method i.e IR and SEM, while pure cellulose was examined by XRD and <sup>1</sup>H NMR. Finally, crude cellulose was designed into a microcrystalline form by acid hydrolysis for a much better surface merits supporting the acetylation reaction resulting in cellulose acetate (CA). Using NMP as a solvent, casting solutions of CA were prepared loaded with graphene oxide (G.O) 0.01, 0.02, 0.05 and 0.1 % (w/v) giving rise to newly developed membranes employed in a reverse osmosis cell. Membranes were characterized by SEM and tested for contact angle values. Decreased contact angles referred to enhanced hydrophilicity explaining the improved permeation rate except for CA membrane loaded with 0.1% GO. The average permeation rate increased for all membranes except for the one loaded with 0.1% GO. Average salt rejection percentage was raised as well for all membranes being 49.3, 53.6, 67.5 and 69.1 %. The incorporation of GO into CA membranes enhanced hydrophilicity, average permeation rate and average salt rejection % of CA membranes derived from date palm fibers.

**Keywords:** Palm fiber, Cellulose acetate, Reverse osmosis, Graphene oxide, CA membrane.

### 1. Introduction

The earth's population has been growing rapidly over the past 150 years, in contrast to a finite and stable supply over geological time. Parallel to the existing problem of water shortage, a problem of over growing agricultural wastes also stands firmly in the route of environmental and economic interests. Lignocellulosic fibers -as an agricultural waste- have a number of well-known advantages over their synthetic equivalents, including the fact that they are carbon dioxide (CO<sub>2</sub>) neutral, environmentally and toxicologically safe, and biologically degradable. Furthermore, natural fibers

are characterized by a huge degree of viability and diversity in their properties. Valorization of agricultural wastes and making the advantage of lignocellulosic fibers not only can solve its accumulation problem but also can employ them for the production of innovative tools that can participate in dealing with other environmental issues such as water related concerns. One of the most outstanding solutions for water problems is membrane technology.

In Egypt, one of the most outstanding wastes is the biomass of date palm trees or what is scientifically referred to as *Phoenix dactylifera*.

\*Corresponding author e-mail: [tamerragab2006@gmail.com](mailto:tamerragab2006@gmail.com).

EJCHEM use only: Received date 26 November 2023; revised date 24 December 2023; accepted date 31 December 2023

DOI: 10.21608/EJCHEM.2023.250836.8909

©2024 National Information and Documentation Center (NIDOC)

During the pruning season, tons of its biomass accumulate in many different spots in Egypt being the world's first producer of dates with the greatest number of palm trees. Biomass of date palm trees includes palm fronds, fibers, foliar and thorns which has been used for centuries and up till now. Palm leaf sheath fiber, sometimes known as "palm fiber," is a naturally occurring, plentiful source of cellulose. Natural fiber, often known as plant fiber, consists mainly of cellulose, hemicellulose, lignin, pectin, and foreign substances joined together [1]. Due to its abundance, availability, non-toxicity, cheap cost, environmental friendliness, biocompatibility, biodegradability, thermal and chemical stability, and derivatizability, cellulose is the most abundant renewable polymer resource currently on the market. [2].

By acetylating cellulose using acetic anhydride, cellulose is chemically changed to become cellulose acetate (CA). It is possible to spin the resulting cellulose acetate compound into fibers, mold it into solid structures, or cast it as a film. Cellulose acetate (CA) is one of the most widespread and applicable polymers. Offering the possibility of chemical modification, CA is a very flexible basement for a variety of chemical reactions that move toward better properties and performances.

By exposing graphite to oxidizing chemicals, which provide the structure of the graphite oxygenated functions and exfoliate the layers, one can create graphene oxide (GO), which has improved water dispersion. Due to the considerable augmentation and improvement of many nanocomposites' mechanical, thermal, and electrical properties, which could result in new applications for many of these nanocomposites, GO has recently become one of the most alluring nanofillers in polymer nanocomposite technology [3].

Lee et al. [4] reported that GO can be responsible for the anti-biofouling effect of nanocomposite membranes in such a way that can change the smoothness of the membrane surface. Because to GO's hydrophilicity and electrostatic repulsion properties, which might potentially cause biodegradation, bioadsorption is not recommended. Water treatment has witnessed a lot of developments over the years. Membrane technology was and still a very applicable, effective and upgrading technique of water treatment. uses selectively permeable barriers, with pores sized to permit the passage of water molecules, but small enough to retain or exclude a large category of particulate and dissolved compounds, depending on their nature either physical or chemical one.

Osmosis is interpreted as the spontaneous or natural passage of water from a medium of higher solute concentration to a medium of lower solute

concentration. According to Osmosis, the solvent naturally travels through a membrane in the course of the typical osmosis process from a low solute concentration (high water potential) to a high solute concentration (low water potential). When the difference in solvent concentration on either side of a membrane is lowered, the Gibbs free energy of the system decreases, which causes the solvent to migrate into the more concentrated solution and creates osmotic pressure [5]. To reverse the natural flow of pure solvent, an external pressure applied which referred to as reverse osmosis.

In contrast to filtration, reverse osmosis uses an osmosis mechanism to move fluid over a membrane. Theoretically, membrane filtration can attain perfect efficiency regardless of variables like the solution's pressure and concentration because the main removal method is straining, or size exclusion. Instead, reverse osmosis uses solvent diffusion across a membrane. Reverse osmosis is most commonly known for its use in drinking water purification from seawater, removing the salt and other effluent materials from the water molecules [6].

## 2. Experimental

### 2.1 Materials & Chemicals

#### 2.1.1 Materials

Agricultural waste (Palm fibers), Palm fibers were taken from a 15 years old palm tree in Menufia governorate, Egypt.

#### 2.1.2 Chemicals

Chemicals used in the extraction process were ethanol ( $C_2H_5OH$ ), sodium hydroxide ( $NaOH$ ), sodium hypochlorite chlorite ( $NaOCl$ ), acetic acid ( $CH_3COOH$ ) and sulphuric acid ( $H_2SO_4$ ), methylene chloride ( $CH_2Cl_2$ ), toluene ( $C_6H_5CH_3$ ), acetic anhydride ( $(CH_3CO)_2O$ ), acetone ( $CH_3COCH_3$ ), n-BuOH ( $C_4H_9OH$ ), potassium persulfate ( $K_2S_2O_8$ ), phosphorus pentoxide ( $P_2O_5$ ), potassium permanganate ( $KMnO_4$ ), hydrogen peroxide ( $H_2O_2$ ), O-phthalic acid ( $C_6H_4(CO_2H)_2$ ), diethyl ether ( $(C_2H_5)_2O$ ), NMP (N,N dimethyl pyrrolidone) solvent, hydrochloric acid (HCl). All the chemicals were reagent grade purchased from Sigma-Aldrich and used without further purification.

### 2.2 Methods

Chemical composition of date palm fibers, moisture and ash contents were determined according to AOAC (1970) [7]. Total carbohydrates were determined after complete hydrolysis according to Debois et al. [8] and the resulting acid hydrolates were examined by paper chromatography using n-butanol/acetone/ $H_2O$  (4:5:1) [9] and aniline phthalate as a spraying reagent [10]. Quantitative determination of separated sugars was carried out according to

Wilson [11]. Chemical characterization of the raw materials and the isolated fractions was detected by FTIR and  $^1\text{H-NMR}$  analysis.

### 2.2.1 Determination of moisture content

Moisture content of the date palm fibers was determined from the weight difference of the samples before and after the drying process.

### 2.2.2 Determination of ash content

Ash content date palm fibers was determined using a muffle furnace at  $800\text{ }^\circ\text{C}$  for 6 hours or till a constant weight was reached.

### Preparation of samples

Palm fibers were prepared for processing by washing with water to remove dust or any impurities and left to dry, cutting into small pieces ranging from 1 to 3 cm in length and well drying at  $60\text{ }^\circ\text{C}$  for approximately 36 h in an electric oven till a constant weight was reached. After complete drying, that pieces were finely ground into small fragments.

### 2.2.3 Dewaxing

Ground palm fibers were soaked in ethanol/toluene mixture (2:1) for 24 h to remove wax, protein and fats.

### 2.2.4 Pulping

The aim of pulping is to break down the bulk structure of the fiber source into the constituent fibers. Dewaxed cellulose was further processed by alkali treatment with NaOH 1 % N in a ratio 1:15 (wt/v) at  $70\text{ }^\circ\text{C}$  for 1 h then filtrated giving crude cellulose residue which was continuously washed with acetic acid and distilled water till neutralization. The dark filtrate resulting from this alkali treatment, containing lignin and hemicellulose, was further treated with ethanol to precipitate hemicellulose.

#### 2.2.4.1 Bleaching of cellulose

To get the crude cellulose bleached, it was treated with sodium hypochlorite solution ( $\text{NaOCl}$  12%) in 1:10 (wt/v) ratio and the mixture was stirred at  $80\text{ }^\circ\text{C}$  for 30 min and filtered then the residue was washed with distilled water.

#### 2.2.4.2 Producing $\alpha$ - cellulose

To produce  $\alpha$ -cellulose, a mercerization process using NaOH 17.5% was performed through a series of successive steps adding NaOH at different interval times while a constant temperature of  $22\text{ }^\circ\text{C}$  was kept via a water bath according to Sun et al. [12].

### 2.2.5 Microcrystalline cellulose (MCC) production

Microcrystalline cellulose or nanoparticles of  $\alpha$ -cellulose were prepared by acid hydrolysis of  $\alpha$ -cellulose with 2% N  $\text{H}_2\text{SO}_4$  in 1:10 (wt/v) ratio and

refluxing at the boiling temperature for 1 h starting from boiling. The suspension was then filtered, washed with distilled water till neutralization and left in air to dry.

### 2.2.6 Acetylation of MCC cellulose

For the acetylation of 20 grams of  $\alpha$ -cellulose, 300 ml of methylene chloride were added to it followed by 5 ml of glacial acetic acid after which 50 ml of acetic anhydride were added then 0.4 ml of concentrated  $\text{H}_2\text{SO}_4$  all at very dry conditions. This reaction mixture was refluxed at  $80\text{ }^\circ\text{C}$  for 4 h after which this mixture was left to cool and filtrated giving a cellulose acetate filtrate which was further dried and ground into powdered cellulose acetate (CA).

### 2.2.7 Preparation of graphene oxide (GO)

Graphene oxide (GO) was prepared according to the modified Hummer's method [13] from palm fibers being ignited giving charcoal via oxidation of graphite powder to attach functional groups.

To prepare GO, 10 gm of palm fibers charcoal was mixed with 5 gm of  $\text{NaNO}_3$  after which 230 ml of cooled  $\text{H}_2\text{SO}_4$  was added to that solid mixture in an ice bath for a controlled low temperature (below  $5\text{ }^\circ\text{C}$ ) then 30 gm of potassium permanganate was added to the mixture which was further moved to a controlled water bath at  $35\text{ }^\circ\text{C}$  for 30 min. Later 500 ml of distilled water was added drop wise to the mixture and the temperature was raised to  $98\text{ }^\circ\text{C}$  after which the mixture was diluted to 1400 ml using warm distilled water. 56 ml of hydrogen peroxide  $\text{H}_2\text{O}_2$  was added to reduce the residual permanganate and manganese dioxide to colourless soluble manganese sulfate. The suspension was filtrated resulting in a yellow-brown filter cake. A filtering was proceeded while the suspension was still warm to avoid precipitation of the slightly soluble salt of mellitic acid formed as a side reaction. After washing the yellow-brown filter cake 3 times by warm water, the graphite oxide residue was dispersed in 32 ml of water to approximately 0.5 solids. The dry form of graphite oxide was obtained by centrifugation followed by dehydration at  $40\text{ }^\circ\text{C}$  over phosphorus pentoxide in vacuum.

### 2.2.8 Determination of low molecular weight carbohydrates

Raw date palm fibers samples were investigated for their content of Low molecular weight carbohydrates according to Debois et al. [8]. The absorbance of the solutions was determined at 390 nm for the hexoses and rhamnose and at 360 nm for the pentoses [11]. Aniline-phthalate reagent and eluting reagent (0.7 ml HCl in 80% ethanol) were

involved in this process and prepared as previously mentioned by Ragab et al. [14].

### 2.2.9 Evaluation of total carbohydrates

Total carbohydrates content for the different fractions were determined qualitatively and quantitatively according to phenol-sulphuric acid method i.e via complete acid hydrolysis [14]. Detection was performed on the spectrophotometer at wave length 490 nm.

### 2.2.10 Determination of monosaccharide constituents form paper chromatography (quantitative determination)

According to Wilson [11], quantitative paper chromatography allows individual determination of mixed sugars in small amounts. The concentration of sugar was determined by spectrophotometry at 360 nm for pentoses and 390 nm for hexoses. The absorbance of the solution is proportional to the concentration of sugar.

### 2.2.11 Chemical characterization of derived fractions, cellulose forms, CA and GO

#### 2.2.11.1 Fourier-Transformed Infrared Spectroscopy (FTIR)

IR spectroscopy is basically employed in order to get information about composition of components and membranes or presence of different functional groups on membrane surface. Samples were characterized on device a Shimadzu FT-IR spectrometer Affinity A1 spectrometer (Bruker Optics, Germany). All spectra were taken at a spectral resolution of  $4\text{ cm}^{-1}$  between wave number range  $4000\text{--}400\text{ cm}^{-1}$ .

#### 2.2.11.2 Nuclear Magnetic Resonance ( $^1\text{H}$ & $^{13}\text{C}$ NMR)

Samples were characterized to detect the modifications developed with each step on device. NMR spectra were measured on a Bruker High Performance Digital FT-NMR spectrometer Avance III 400MHz (Bruker Optics, Germany).

#### 2.2.11.3 Fourier-X-ray diffraction (X-RD)

X-RD technique provides such a way to investigate the structural characteristics or crystallinity of polymer or nano-composite membrane. XRD is the best tool as it is a non-destructive technique. Diffraction patterns were obtained using a Phillips X-ray diffractometer.

#### 2.2.11.4 Scanning Electron Microscopy (SEM)

Morphology and topography of processed frond fractions, progressed cellulose forms and prepared membranes surfaces, were all investigated by SEM technique. Samples of processed palm

fronds, cellulose forms and prepared membranes were examined through SEM analysis via a Quanta FEG 250 device with an accelerating voltage conducted at 10 kV. Cellulose samples were gold coated using a Hitachi coating unit IB-2 coater under a high vacuum, 0.1 Torr, high voltage, 1.2 kV and 50 mA.

#### 2.2.11.5 Transmission electron microscopy (TEM)

Transmission electron microscopy (TEM) by TECNAI G2 20 S-TWIN device was used to determine the morphology and dimensions of the micro and nano-crystalline cellulose. The basic building blocks of membrane can also be examined by (TEM). Quantitative information of particle, size distribution, morphology, and grain size can be obtained as well. Samples were prepared by placing few drops of the nanoparticles suspension on carbon coated copper grid, followed by allowing the solvent to evaporate slowly before recording the TEM image.

### 2.2.12 Membrane preparation

Membranes were prepared according to wet phase inversion by immersion precipitation technique. Dried CA prepared from palm fibers was dissolved in NMP (N, N dimethyl pyrrolidone) solvent, stirred using a mechanical stirrer at  $30^\circ\text{C}$  according to ratios illustrated in (Table. 1), till a homogeneous solution was reached. The mixture was further moved to a refrigerator and left-over night to get rid of any air bubbles. Preceding to membrane casting, the casting glass sheet was cleaned by tap water and acetone then dried before use. The homogeneous solution was sprinkled and casted onto a dry clean glass sheet using a  $200\ \mu\text{m}$  automatic casting knife. The casted polymer matrix was left for 45 s for partial solvent evaporation then immersed into a water coagulation bath at  $20^\circ\text{C}$ . The as-cast membrane was peeled off from the glass plate and moved toward coagulation tap water bath for immersion precipitation at  $20 \pm 2^\circ\text{C}$ . After solidification, the membranes were soaked in deionized water for 24 h before performance testing.

**Table 1**

Compositions of the casting solutions % (wt/v) for the prepared membranes

Membrane	CA	GO	NMP
CA	20	0	80
CA+ GO 0.01%	20	0.01	79.99
CA+ GO 0.02%	20	0.02	79.98
CA+ GO 0.05%	20	0.05	79.95
CA+ GO 0.1%	20	0.1	79.9

### 2.2.13 Characterization of the prepared membranes

#### 2.2.13.1 SEM examination

Scanning by electron microscope (SEM) was incorporated as a tool for identifying the morphological characters of the concerned membranes. Testing was achieved using Quanta FEG device in the National Research Centre, Egypt.

#### 2.2.13.2 Physical appearance & thickness

Membranes were examined for their relative strength and appearance besides their initial casting thickness (ICT) values and the final casting thickness (FCT) ones.

#### 2.2.13.3 Determination of contact angle

Contact angle measurements were performed to investigate the hydrophilicity of the prepared membranes using the sessile drop method [15].

### 2.2.14 Membrane performance (permeation and salt rejection rates)

Performance of the prepared membranes was evaluated by detecting their permeation and salt rejection rates. The concerned membranes were tested via Sterlitech HP4750 Stirred Cell (a dead-end cell filtration system) to investigate the permeation flow and salt rejection rates. A pressure of 10 bars was applied for an appropriate permeation flow.

A solution of NaCl with a concentration of 2000 ppm was employed as the feeding solution that can be considered as a representative for brackish water containing a high concentration of chloride ( $\text{Cl}^-$ ) ions with an average concentration of 2000 ppm [16]. The feeding solution passed through a membrane active area of  $14.6 \text{ cm}^2$  in the pressurized flow-through system. Both permeation rate and salt rejection % were determined according to the following equations;

$$\text{Permeation rate (J)} = \frac{Q}{A \times t} \quad (\text{eq. 1})$$

Where  $J$  is the permeation rate in  $\text{L/m}^2\text{h}$ ,  
 $A$  is the area of the membrane on which pressure is applied ( $\text{m}^2$ ),  
 $Q$  is the volume of permeate (L)  
 and  $t$  is the time of permeation (h)

$$\text{Salt rejection \%} = \left( \frac{C_f - C_p}{C_f} \right) \times 100 \quad (\text{eq. 2})$$

Where  $C_p$  is the concentration of permeate solution  
 And  $C_f$  is the concentration of feed solution [17].

Concentrations for both permeate and solutions were measured by Cond 330i (WTW 82362 Welheim) device.

#### Statistical Analysis

A repeated measure one-way analysis of variance (ANOVA) was used for the statistical analysis, followed by the least significant test for multiple comparisons. At  $p < 0.05$ , the effects were deemed significant. Results were given as the mean  $\pm$  standard error.

## 2. Results and discussion:

### 3.1 Chemical pulping of palm fibers

Complex, dynamic cellular structures called plant cell walls are necessary for a plant's growth, development, physiology, and adaptation. Aside from water, that wall's major constituents are cellulose fibers, lignin, a three-dimensional polymer that holds the cellulose fibers together, and hemicelluloses, which are smaller branched carbohydrate polymers. Breaking down the fiber's bulk structure is the purpose of pulping. When cellulose fibers are pulped, heat and chemicals are introduced to break down the lignin that holds them together without substantially damaging them. Due to its degree of polymerization and partly crystalline structure, cellulose can only be dissolved in particular specific complexes and extremely concentrated acid and base. As a result, it is difficult to dissolve in conventional solvents. The chemical composition (Fig. 1) of date palm fibers was determined according to the recommended methods.

Fibers from date palm tree (*Phoenix dactylifera*)-especially fibers extracted from the leaf sheath and stem- were chemically pulped and treated in order to figure out a chemical characterization that would give a clear perspective of how far good would be the trend of this biomass valorization and to what extent could this be ever possible. Palm family fibers possess similar compositions. As natural composites, palm and other fibers require binders (particularly lignin and hemicellulose) to hold several cells together [18].

Chemical pulping of date palm fibers here came up with results of interest. Herein, cellulose content of fibers was found to be 60.23 % that is far from that value reported by Alain Bourmaud et al. [19] reporting that cellulose content of leaf sheath fibers bundles was  $45.1 \pm 3.4\%$ . Sbai et al. [20] indicated that cellulose content of palm fibers was 35%. Tonghua

Zhang et al. [18] also informed that palm fiber content of cellulose was to be 28.18%.

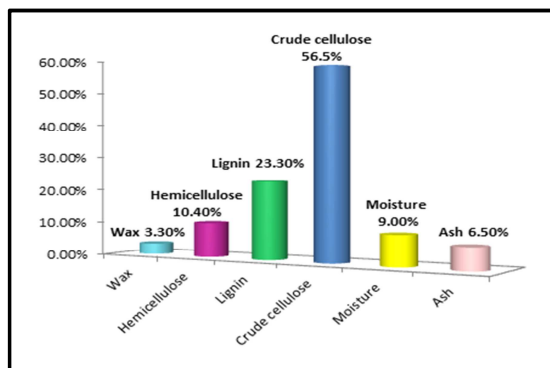


Fig. 1 Chemical constituents of palm fiber

Concerning this work, lignin content of date palm fibers was found to be 44.30% that agreed with Pradeep P. and Edwin R. D.J. [21] reporting that lignin content of palm leaf sheath fibers was 45% which also agreed with a lignin content of 44.07% detected by Tonghua Zhang et al. [18] but disagreed with Sbiaiet al.[20] who characterized lignin in palm fibers to be about 27% [21] supported by Bourmaud A. et al. [19] with a lignin content around  $16.9 \pm 3$  for leaf sheath fibers bundles.

Chemical pulping of date palm fibers investigated here resulted in a hemicellulose content of 10.4% which apparently varied from values published before for the same fraction, as Sbai et al. [20] found that hemicellulose content was 28% while Tonghua Zhang et al. [18] reported that it was 20.06%. A higher hemicellulose content was revealed to be  $27.7 \pm 1.5$  by Bourmaud A. et al. [19].

Reneta Y. et al. [22] researched both palm spikelets and stalk fibers and reported that ash content of them was to be 7.07 and 10.58% respectively while the ash content investigated here for date palm fibers was found to be 2.5%. Despite this disagreement with Reneta Y. et al. [22], ash content detected here as 2.5% obviously agree with that result reported by Abdul Khalil H. P. S. [23] for oil palm fronds valued as 2.4%. In addition, ash content of palm sheath fibers investigated by byTonghua Zhang et al. [18] was  $1.7 \pm 0.1$ .

Derived crude cellulose inhere was bleached to be as 44.93 % declaring the additional amounts of lignin and other extra color giving substances. The bleached cellulose went through mercerization for highly purified alpha cellulose evaluated as 31.90 % which was not so far from that reported by Tamer I. M. Ragab et al. [24]. The outcome  $\alpha$ -cellulose content was strongly hydrolyzed by 2% N  $H_2SO_4$  giving rise to microcrystalline cellulose as much as

24.61 % while when further acetylated, the resultant cellulose acetate was as 10.80 %.

### 3.1.1 Total carbohydrates

Total carbohydrates were determined after complete hydrolysis according to Debois et al. [8] where sugars and strong acid condense with reagents (e.g. phenol) in hot conditions to yield colored complexes so according to phenol-sulphuric acid method, and by utilising paper chromatography, n-butanol/acetone/ $H_2O$  (4:5:1) and aniline phthalate as a spraying reagent [10], the resultant acid hydrolates were studied. The quantitative analysis of isolated sugars was done in accordance with Wilson [11] and results are described in (Table. 2).

Table 2

Total carbohydrates in the investigated samples

Sample	Total carbohydrate content
Raw fiber	23.4 %
Crude cellulose	23.95 %
Bleached cellulose	37.5 %
Alpha cellulose	19.5 %
MCC	24.5 %
CA	12 %
Hemicellulose	21.4 %
Lignin	11.45 %

### 3.1.2 Monosaccharide constituents from paper chromatography

According to Wilson [11], the paper was immersed in Partridge's aniline hydrogen phthalate reagent. The color was eluted of from the paper with alcoholic hydrochloric acid. The colored spots from the paper were segmented and eluted with 4 ml of the eluting agent (0.7 ml HCl in 80% ethanol), the concentration of sugar was determined byspectrophotometry at 360 nm for pentoses and 390 nm for hexoses. The absorbance of the solution was proportional to the concentration of sugar and the results are showed as following in (Table. 3).

### 3.1.3 Bleaching crude cellulose:

Using bleaching agent during natural fiber treatment, always aims at removing color and increasing whiteness of the fibers for a more convenient employment. Chemical bleaching was performed using Sodium hypochlorite (NaOCl 12%) that can attack cellulose fibers removing remaining lignin and other substances responsible for the color. NaOCl can selectively oxidize the conjugated non-aromatic groups that are responsible for absorbing visible light in lignin. Chlorine performs aromatic substitution to replace hydrogen on the aromatic rings of lignin, oxidises pendant groups to carboxylic acids, and adds cross C=C bonds to the side chains of lignin [25].

**Table 3** Monosaccharide constituents for fractions of date palm fibers

Sample	Glucuronic acid	D-glucose	Arabinose	Xylose	Rhamnose
Raw palm fibers	6%	36 %	26 %	32 %	Traces
Crude cellulose	4 %	41 %	19 %	36 %	---
Bleached cellulose	5 %	74 %	19 %	traces	---
Alpha cellulose	4 %	94 %	traces	---	---
MCC	2 %	97 %	traces	---	---
Hemicellulose	3 %	15 %	61 %	20 %	---
Lignin	3 %	6 %	traces	traces	---
Water extract	9 %	62 %	18 %	11 %	---

### 3.1.4 Alkali treatment

It is widely accepted that cellulose must have a significant number of its inter- and intra-molecular hydrogen bonds broken in order to disintegrate.

### 3.1.5 Alpha cellulose extraction

At strong alkali treatment using NaOH (17.5), cellulose becomes swollen and after swelling, cellulose contracts after washing to produce a newallomorph. Mercerization of cellulose fibers results in the reorganization of cellulose structure by rupturing hydrogen bonds and weakening Van der Waal forces in the cellulose chain to  $\alpha$ -cellulose [25].

## 3.2 Characterization of fractions

### 3.2.1 Fourier-Transformed Infrared Spectroscopy (FTIR)

#### Hemicellulose

**Fig. 2(A)** represents the IR spectrum for hemicellulose. The absorption at  $1633\text{ cm}^{-1}$  is principally associated with absorbed water, since the hemicelluloses usually have a strong affinity for water, and in the solid state these macromolecules may have disordered structures which can easily be hydrated [26]. The band at  $1032\text{ cm}^{-1}$  is attributed to the C–O, C–C stretching or C–OH bending in hemicelluloses [27]. The sharp band at  $874\text{ cm}^{-1}$ , which corresponds to the C1 group frequency or ring frequency, is characteristic of  $\beta$ -glycosidic linkages between the sugar units [28]. An intensive band at  $1456\text{ cm}^{-1}$  corresponds to the C=O stretch of carboxylic anions (salt) for uronic acids in hemicelluloses [27]. A small peak refers to stretching vibration of C=O in acetyl group at  $1742\text{ cm}^{-1}$ . The occurrence of a small band at  $1530\text{ cm}^{-1}$  refers to an aromatic skeletal vibrations of benzene ring that is undoubtedly due to the presence of small amounts of associated lignin in the hemicelluloses. At  $2925\text{ cm}^{-1}$  there is C-H symmetric vibrations. A band at  $874\text{ cm}^{-1}$  refers to -CH rocking vibrations characteristic of cellulose backbone and pyranose ring. The broad band at  $3696\text{ cm}^{-1}$  represents the hydrogen bond in -OH group [29].

#### Lignin

The absorption at  $1122\text{ cm}^{-1}$  is principally associated with cyclic ether. The stretching vibration absorption of cyclic ether large ring stretching refers to DODO inter monomeric lignin linkage [30]. An absorption for carbonyl group C=O in lignin appears at  $1790\text{ cm}^{-1}$  while the peak at  $1456\text{ cm}^{-1}$  represents bending vibrations of phenolic OH. The peak at  $2925\text{ cm}^{-1}$  a peak refers to C-H stretching. The bands at  $3778$  and  $3911\text{ cm}^{-1}$  refer to C-H stretching vibrations of methoxy groups but the peak at  $3696\text{ cm}^{-1}$  represented hydrogen bond in -OH group. As presented in **Fig. 2(B)**, the absorptions from  $1500$  to  $1600\text{ cm}^{-1}$  are attributed to aromatic skeleton vibrations as a peak at  $1604\text{ cm}^{-1}$  is caused by aromatic nucleus vibration while the absorption at  $1025\text{ cm}^{-1}$  is representing skeletal vibrations C-O [31].

#### Crude cellulose

A broad band at  $3434\text{ cm}^{-1}$  representing -OH stretching of the hydrogen bond, at  $2925\text{ cm}^{-1}$  there is an asymmetric stretch of methyl and methylene groups. There is a band for C–H vibrations of a polysaccharide or OH of  $\text{CH}_2$  bending at  $1456\text{ cm}^{-1}$ . The band at  $1634\text{ cm}^{-1}$  refers to adsorbed  $\text{H}_2\text{O}$  while a band at  $875\text{ cm}^{-1}$  refers to -CH rocking vibrations characteristic of cellulose backbone and the  $\beta$ -glycosidic linkages between glucose units. At  $1044\text{ cm}^{-1}$ , a band may represent C–O–C stretching vibrations of the polysaccharide or ring stretching as appearing in **Fig. 2(C)** [32].

#### Microcrystalline cellulose (MCC)

The FTIR spectrum of MCC (**Fig. 2(D)**) showed a peak at  $1054\text{ cm}^{-1}$  due to C–C ring stretching band and a C–O–C glycosidic ether band at  $1158\text{ cm}^{-1}$  while the peak at  $1425\text{ cm}^{-1}$  refers to the scissoring motion of the - $\text{CH}_2$  rocking vibrations characteristic of cellulose backbone and the  $\beta$ -glycosidic linkages between glucose units [33]. The bending vibration of O-H  $\text{cm}^{-1}$  due to absorbed water appears at  $1632\text{ cm}^{-1}$  [34]. The peak at  $2925\text{ cm}^{-1}$  represents C-H stretching [35] while the one at  $3429$

$\text{cm}^{-1}$  represents O-H stretching (axial vibration) of intramolecular hydrogen bonds for cellulose [36].

#### Cellulose acetate

The FTIR spectrum of cellulose acetate as shown below in **Fig. 2(E)**, showed the difference bands prior to and following fiber acetylation, with the largest variations linked to the finger print region between 1900 and 600  $\text{cm}^{-1}$ . The appearance of a band at 1758  $\text{cm}^{-1}$ , which was proceeding from a broad CO carbonyl peak for bound acetyl groups, is the primary difference between the spectra of treated and untreated fibers. Moreover, a small band at 1435  $\text{cm}^{-1}$  referred to C-H bond in OCOCH<sub>3</sub> group [37]. Peaks in the 1840-1758  $\text{cm}^{-1}$  and 1700  $\text{cm}^{-1}$  regions vanished, indicating that the product is free of unreacted acetic anhydride and its byproduct, acetic acid [38]. Bands at 1050  $\text{cm}^{-1}$ , proceeding from C-O alcoholic stretch and at 1439  $\text{cm}^{-1}$  from C-H from cellulose and hemicelluloses, were observed [39]. A strong band at 1064  $\text{cm}^{-1}$  is due to the C O C pyranose ring skeletal vibration, while the amorphous component of cellulose was assigned to the band at 897  $\text{cm}^{-1}$  [40]. The band supposed to be at 1760-1840  $\text{cm}^{-1}$  from acetic acid was absent meaning that the cellulose acetate samples were free from acetic acid.

#### 3.2.2 NMR (Nucler Magnetic Resonance)

##### <sup>1</sup>H-NMR of CA palm fibers

<sup>1</sup>H NMR spectrum for cellulose acetate shown in **Fig. 3(A)**, revealed that cellulose extracted from palm fibers was converted into cellulose acetate due to the appearance of methyl protons (CH<sub>3</sub>) group belonging to acetyl groups in the range of 1.9-2.1ppm while the range of the seven anhydrocellulose proton absorption was 3.1-5.1 ppm.[41].

##### <sup>13</sup>C-NMR of CA of palm fibers

<sup>13</sup>C-NMR presented in **Fig. 3(B)** showed significant signals appearing at  $\delta$  170.7 referring to

carbonyl carbon plus that at  $\delta$  20.53,  $\delta$  20.65, 21.04 and  $\delta$  21.51 assigned for methyl carbons.

#### 3.2.3 X ray diffraction (XRD)

Both crystalline and pre-crystallization (alpha and microcrystalline) cellulose of palm fibers were subjected to X ray diffraction in order to figure out the crystallinity index. A Phillips X-ray diffractometer was the device in use for reporting the diffraction patterns. Carl von Nägeli [42] discovered cellulose's crystalline structure for the first time in 1858. The following equation was used to calculate the crystallinity index (CI) using Segal's empirical methodology.

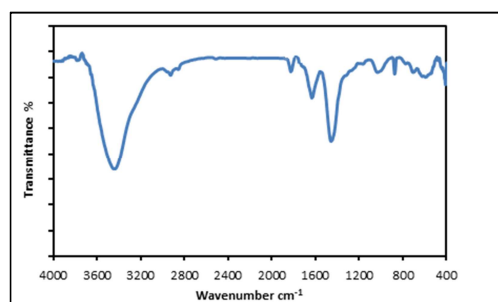
$$\text{CrI \%} = (I_{002} - I_{\text{am}}) / I_{002}$$

where  $I_{002}$  is the peak's intensity value of micro crystalline cellulose ( $2\theta = 22.3^\circ$ ), while  $I_{\text{am}}$  is the intensity of the peak value for the amorphous alpha cellulose.

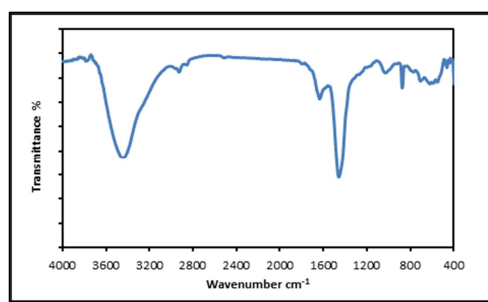
The diffractograms of both alpha cellulose and microcrystalline cellulose (MCC) of palm fiber presented in **Fig. 4(A)** revealed two well-defined and narrow peaks with the Bragg angles ( $2\theta$ ) due to formation of perfect crystals form microcrystalline palm fiber cellulose. For microcrystalline cellulose of palm fibers, crystallinity index (CI) was 31.15% while for the pre-crystallization form of cellulose (alpha cellulose) it was 26.51% reflecting the increased degree of crystallinity along with microcrystalline development (**Fig. 4(B)**).

### 3.3 Characterization of graphene&graphene oxide

#### 3.3.1FTIR for graphene&graphene oxide



(A)



(B)

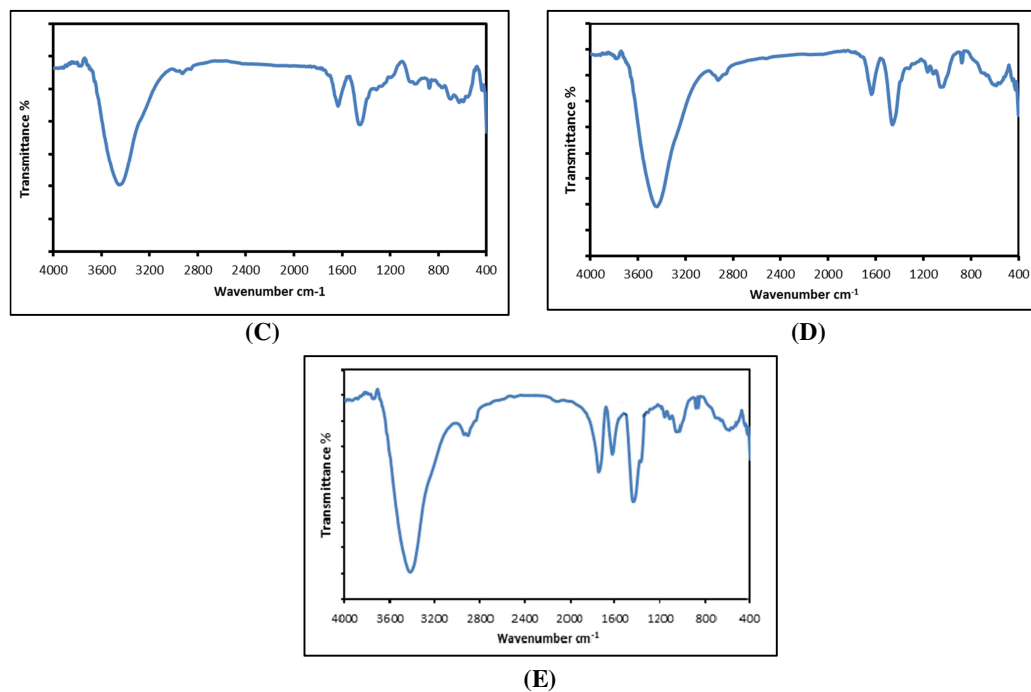


Fig.2 IR spectra for palm fibers and its fractions (A) Hemicellulose, (B) Lignin, (C) Cellulose, (D) Mcc cellulose and (E) Cellulose acetate

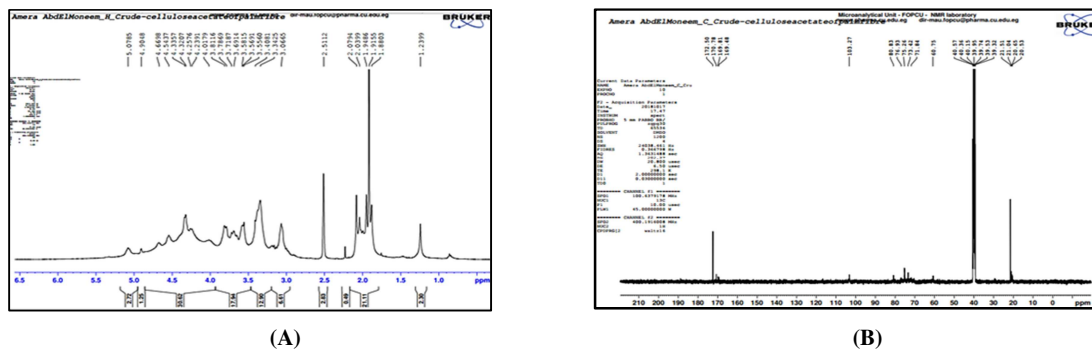


Fig. 3. NMR for CA of palm fiber (A) <sup>1</sup>H NMR and (B) <sup>13</sup>C NMR

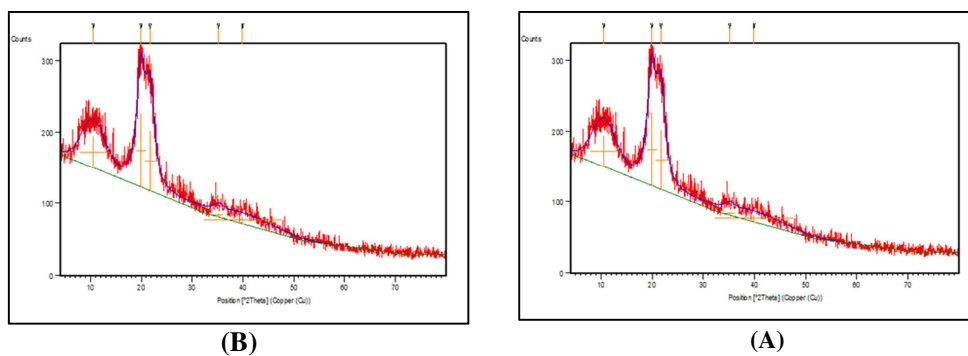


Fig. 4. XRD Diffractogram for palm fiber(A)  $\alpha$ -cellulose and (B) MCC cellulose

**Fig. 5(A)** represents a band at  $3000\text{--}3660\text{ cm}^{-1}$  that referred to OH groups belonging to  $\text{H}_2\text{O}$  molecules adsorbed on GO. The peak at  $1634\text{ cm}^{-1}$  referred to the stretching vibration of  $\text{C}=\text{C}$  of the graphitic basal plane [42]. A peak at  $1700\text{ cm}^{-1}$  is attributed to the stretching vibration of  $\text{C}=\text{O}$  of carboxylic acid and carbonyl groups presented at the boundaries of graphene oxide. The extended pulses of  $\text{C}-\text{O}$  of carboxylic group appeared at  $1220\text{ cm}^{-1}$  while that of  $\text{C}-\text{OH}$  of alcohol existed at  $1079\text{ cm}^{-1}$  [43]. According to the IR spectrum of graphene (an intense peak appeared at  $1410\text{ cm}^{-1}$  is assigned to the vibrational deformation mode of  $\text{O}-\text{H}$  groups present in graphene while in **Fig. 5(B)**, the intensity of this peak greatly declined declaring the oxidation of graphene to graphene oxide.

### 3.3.2 X ray diffraction (XRD)

The XRD pattern of graphene oxide prepared from palm fibers is presented in **Fig. 6 (B)** showing the diffraction peak at  $2\theta = 12.81^\circ$  which agreed with that for date palm fronds (at  $2\theta = 12.68^\circ$ ) revealed by Tamer Ragab et al. [24]. The obtained value was also and near that detected at  $2\theta = 11.72^\circ$  for graphene oxide prepared from sugarcane bagasse [44]. Chemical oxidation of graphene by Hammer's method led to the decline in the main peak's intensity, compared to that of parent graphene (**Fig. 6(A)**), which was between  $2\theta$  of almost  $26^\circ$  and  $30^\circ$ .

### 3.3.3 Scanning Electron Microscope (SEM):

Electronic examination by scanning the different stages of palm fibers going through chemical and morphological changes during the gradient process it experienced. Scanning of raw, bleached fibers and the mcc was achieved using Quanta FEG device in the National Research Centre.

#### Raw palm fibers

The micrograph of untreated palm fibers (**Fig. 7(A)**) displayed a considerable amount of non-

cellulosic components scattered over the surface. The untreated raw form of palm fibers showed a typical complex outer structure due to the presence of lignin, hemicellulose and waxes surrounding the main fiber bundles meanwhile, the neat order and compact ligocellulosic internal structure were clearly observed. Cracks and small cavities appeared on the surface [45].

#### Bleached fibers

A more uniform and clean structure of long cellulose fibers (**Fig. 7(B)**) appeared after bleaching with  $\text{NaOCl}$  12% leading to a very ideal homogenous appearance. Removal of non-cellulosic constituents was procedure via treating with sodium hydroxide ( $\text{NaOH}$ ), lignin was via depolymerization and complex formation, eliminated. The hemicellulose was hydrolyzed and made water soluble upon further treatment with alkali, aiding in the defibrillation of the fibrils. Destruction of the natural fiber bundles after bleach treatment evolved a diameter reduction. This reduction was mainly attributed to the separation of the fibers cell wall due to the removal of hemicellulose and lignin.

#### Micro and nano-crystalline cellulose fibers

The significant characteristics in the micrograph of nanocellulose were refinement of the fiber structure (**Fig. 7(C)**) coupled with additional reduction in its diameter and intermittent break down in fiber structure in its axial direction. Because all amorphous areas of semi-crystalline cellulose were removed, only nanoscale rod-like crystals and a few sphere-like structures remained, greatly reducing the diameter and size of the refined cellulose fibrils. A part of the powdered cellulose was in the nano form having sizes about 228.9, 267.1, 291.8 and 314.6 nm, while Some particles had a diameter of  $3.466\text{ }\mu\text{m}$  and the length of 12.95, 21.43 and  $25.59\text{ }\mu\text{m}$  of rod like cellulose micro-structure. The elimination of lignin

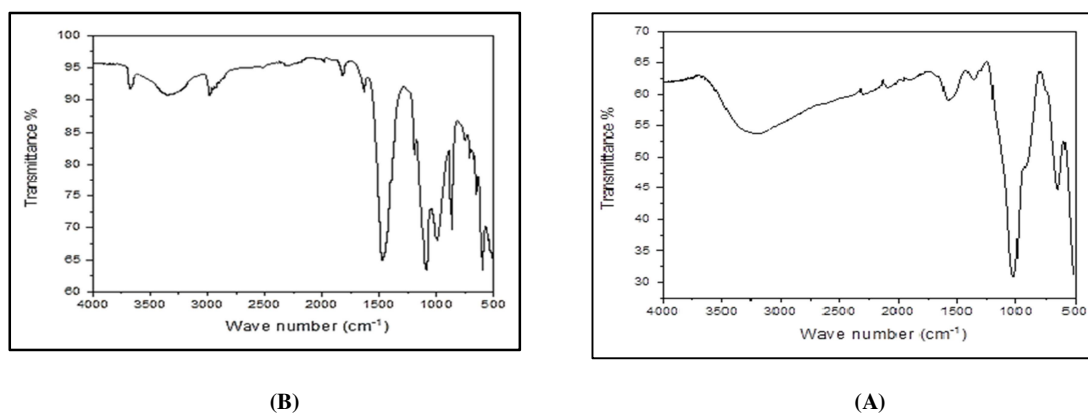


**Fig. 5.** FTIR spectrums for prepared (A) graphene and (B) graphene oxide from palm fiber

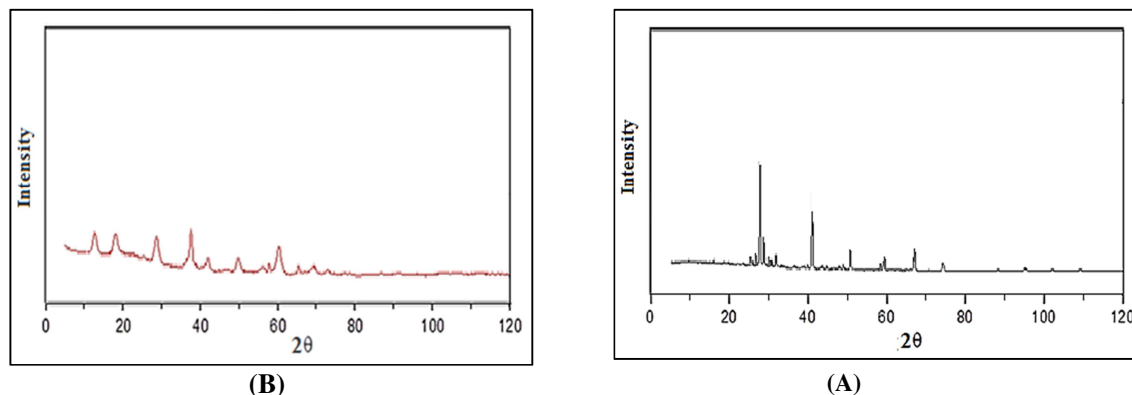


Fig. 6. XRD patterns for (A) graphene and (B) graphene oxide from palm fiber

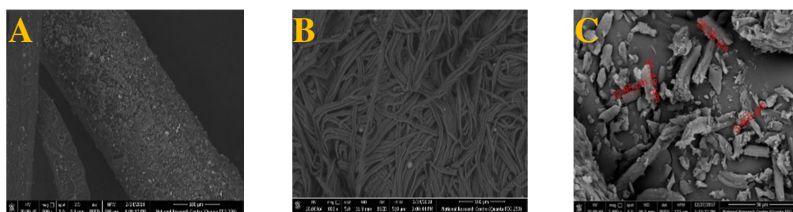


Fig. 7. SEM images for (A) Raw, (B) Bleached and (C) MCC of palm fibers respectively

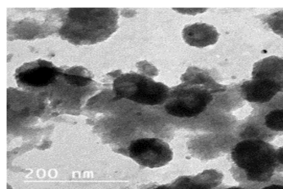


Fig. 8. TEM images of microcrystalline cellulose

and hemicellulose following bleaching and alkali treatment was primarily blamed for the separation of the fiber's primary cell wall, which resulted in size decrease.

### 3.3.4 (TEM)

According to the high resolution TEM images (Fig. 8) of crystalline cellulose (MCC) from date palm fibers, smaller spherical crystalline form about 200-500 nm in size appeared. These cellulose spheres may have originated from self-assembled short cellulose rods through interfacial hydrogen bonding and/or the preparation procedure. Due to additional hydroxyl groups exposed on the surface, the aggregation of nanocrystalline cellulose demonstrated that cellulose chains exhibit significant hydrophilic interactions and intermolecular hydrogen bonds.

### 3.4 Characterization of casted membranes

Membranes were casted and prepared according to phase inversion technique. This technique depends on the method of inducing phase separation, which transforms a polymer from a liquid dispersion into a solid, by the carefully controlled interaction of solvent and nonsolvent solutions [46].

Participation of NMP as a solvent could have contributed to the porosity and pore size's changes during membrane's preparation. WoongGi Lee et al. [47] concluded that NMP present in the CA polymer was removed by the high pressure of water there in addition, the penetration of water molecules through the weakened parts of the CA polymer was responsible for the development of pores in the membrane structure. NMP is known for its plasticization effect in the concerned polymer. Being a good solvent and acting as a plasticizer, the use of

NMP as a solvent could result in a fairly low accepted viscosity [48]. NMP evaporates slower than various other solvents because of its higher vapor pressure. As a result, NMP remains in the CA membrane, causing an increase in the plasticization effect. The region weakened in the polymer by NMP, is exposed to water pressure as an external physical force and the polymer chains are loosened by NMP thereby producing a porous region [47]. To keep the viscosity of the polymer solution in levels suitable for membrane casting, the concentration of CA was decided to start with 20 % while the added GO percentages were 0.01, 0.02, 0.05 and 0.1 % (w/v) respectively as presented previously in **table 1**.

### 3.4.1 Chemical characterization

#### 3.4.1.1 SEM Examination

Electron microscopic scanning (SEM) participated in the morphological characterization of the prepared membranes. Testing was achieved using Quanta FEG device in the National Research Centre. Shots taken were presented below in **Fig. 9**.

SEM views (**Fig. 9 a**) of neat CA membrane revealed the existence of atypical finger-like structure with few macrovoids in the cross-section area. Those finger-like structures go along with the whole membrane thickness. It is believed that asymmetric membranes are formed as a result of rapid precipitation (short gelation periods) with a "finger" like structure. Highly porous with a relatively very small dense layer, was also a characteristic feature of the cross-section scanning. Shots showed also that the crude CA membrane of palm fibers, was pore free at the skin surface while the bottom (glass side) surface was highly porous. SEM results of CA (palm fiber)

doped with graphite oxide 0.01 % membrane showed much more and enlarged pores than those noticed in SEM results of crude CA membrane as seen in **Fig. 9 b**. Pores appearing after the addition of graphite oxide by 0.02%, had larger sizes and increased pore diameter as 0.1331, 0.2952, 0.3320, 0.4216 and 0.6080nm for the top views in addition to those of the bottom views reaching more than 0.2093 nm (**Fig. 9 c**). Successive increase in the load of GO led to further increase in macrovoidal size and diameter of pores at the concentration of 0.05% of GO, pores were also enlarged to be as 0.2759, 0.3011, 0.7834, 0.8345, 0.6658  $\mu\text{m}$  as appearing in **Fig. 9 d**. In case of loading the casting solution with 0.1% of GO, decreased size of macrovoids was noticed and smaller pore size appeared as well according to **Fig. 9 e**. The resulting pores got a little dimensioned some of them were as large as 0.1503, 0.3632, 0.4503, 0.2335, 0.2861 nm. The minimized macrovoidal size might have been due to increase in viscosity ascribed to the GO conc.

#### 3.4.1.2 IR spectroscopic examination,

The modified chemical structure of CA membranes was proved via IR spectroscopy as shown in **Fig. 10**. The significant peaks for CA were presented at almost  $1085\text{ cm}^{-1}$  proceeding from C–O alcoholic stretch from C–H from cellulose. The IR pattern showed a peak at  $1225\text{ cm}^{-1}$  for the expansion vibration of C–O–C while the peak at  $1371\text{ cm}^{-1}$  referred to C–CH<sub>3</sub> stretching. A peak at  $1722\text{ cm}^{-1}$  stood for the C=O group from acetyl group. Peaks at  $2936$  and  $3427\text{ cm}^{-1}$  related to the stretching vibration of the C–H and O–H bands, respectively [49].

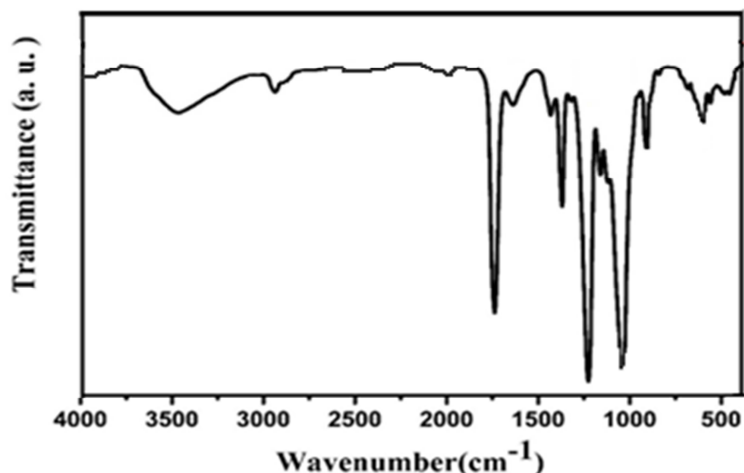


**Fig. 10.** IR spectrum for CA membrane loaded with GO

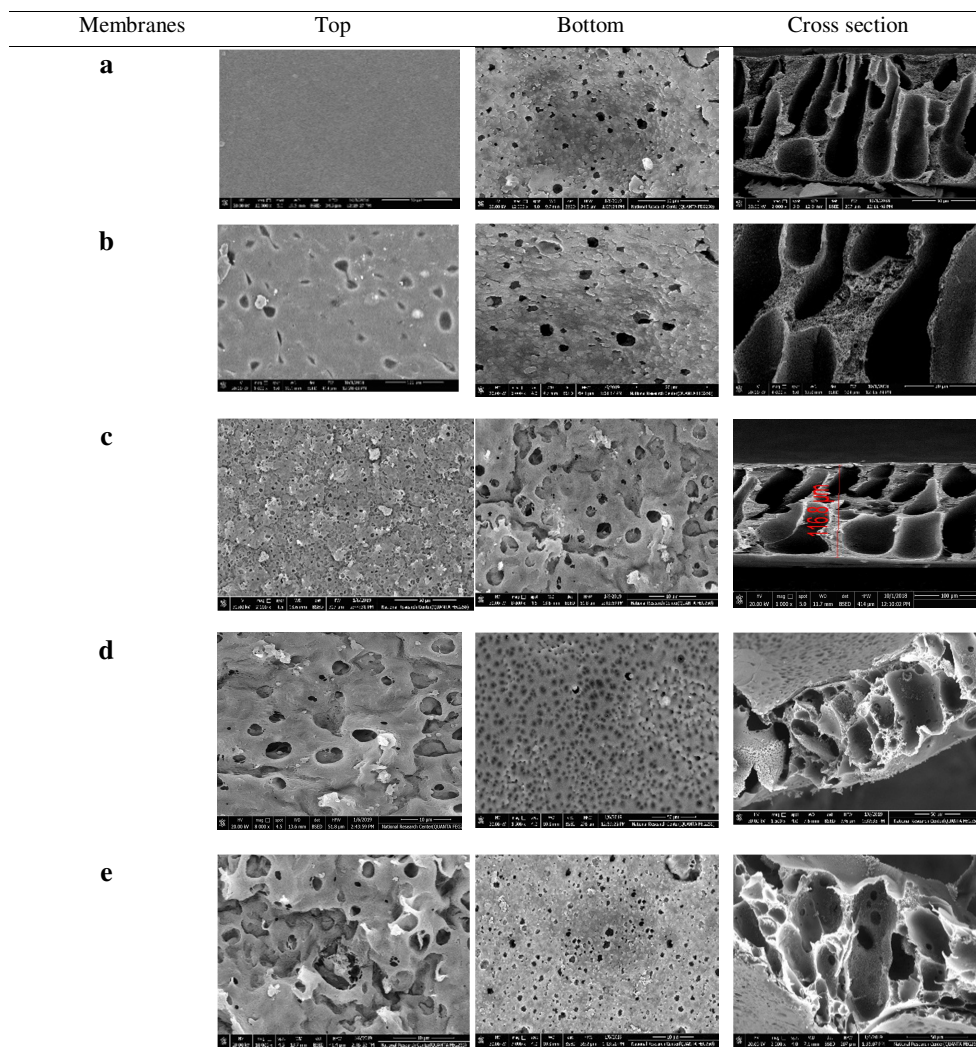


**Fig. 9** SEM images of the top, bottom and cross-sections for (a) Crude CA, (b) CA+GO 0.01%, (c) CA+GO 0.02%, (d) CA+GO 0.05% and (e) CA+GO 0.1% membranes

### 3.4.2 Physical appearance

The produced membranes containing GO, showed good physical appearance with no cracks but relative strength which can be due to the presence of two types of dominating interactions, including hydrogen bonds and the Van der Waals interaction between the C=O groups from CA and -OH and -COOH groups from GO.

The rate of mixing between water as a non-solvent and NMP as the meant solvent during phase inversion, is believed to be increased due to hydrophilic GO particles, resulting in a relatively lean top surface [50]. As a result, a decrease in the thickness of the membrane was noticed approving with former opinions relating the decline of thickness with the involvement of GO particles [51]. Increase in the load of GO into the membrane's casting solution,

was responsible for growing up viscosity causing a decrease in the rate of mass transfer concerning water (the non-solvent).

The initial casting thickness (ICT) was found to be 200  $\mu\text{m}$  for almost all the prepared membranes, while the final casting thickness (FCT) was turned to be approximately 90  $\mu\text{m}$ .

#### Membrane performance

Filtration is a physical and chemical process that is affected by the filter medium, the water, and the flow rate. Prepared membranes of CA loaded with GO, were tested for their performance and characteristics. Detection of contact angle values was proceeded to determine hydrophilicity of each concerned membrane. Results are presented in **table 4**.

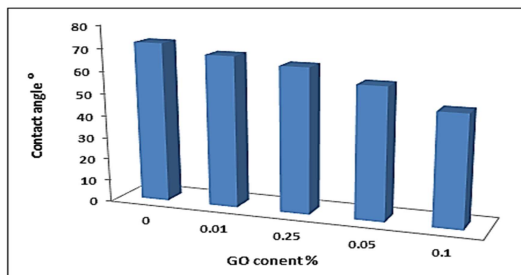
**Table 4.** Parameters of the tested prepared membranes and their characteristics

Membrane	Contact angle	Permeation rate (L/m <sup>2</sup> h.bar)	Salt rejection %
CA	72	0.009±0.0001	44±0.01
CA+G.O 0.01%	68	0.013±0.002	49.3±0.04
CA+G.O 0.02%	65	0.02±0.0013	53.6±0.03
CA+G.O 0.05%	59	0.026±0.002	67.5±0.04
CA+G.O 0.1%	50	0.024±0.0015	69.1±0.016

### 3.4.3 Contact angle measurements

Sessile drop method was approached for the detection of contact angle values for the prepared membranes which reflects directly their hydrophilicity. During the preparation of GO, Utilizing KMnO<sub>4</sub>, graphite was oxidized to add hydrophilic functional groups to its surface. Surface chemistry of the membrane governs the surface interactions with water molecules. Having a number of functional groups with oxygen, such as carboxyl, epoxy, and hydroxyl groups, GO supported the negative character of the membrane's surface leading to increased membrane-water molecule contact leads to an increase in hydrophilicity. Concerning hydrophilicity, GO move toward the top layer when being prepared by phase inversion as a result of the GO's superior attraction of OH groups leading to lower water contact angles. Lower contact angles between water and GO incorporated membranes, might have arisen from the messy dispersion of GO into the membrane's surface, in addition to the bad compatibility and adhesive forces between GO and CA as the polymer of choice for the membrane in case of increasing the filler content.

Enhancement of the membrane's hydrophilicity was determined by the decrease in the water contact angle of the CA/GO membranes from 72° for pure CA membrane) to 68° for CA/GO 0.01%. With continuous adding of GO to 0.02%, water contact angle also decreased to 65° and 59° when 0.05% GO was added respectively (**Fig. 11**). Further increase led to dimensioned angle as well indicating that 0.1% GO could have decreased the water contact angle up to 50° meaning the best hydrophilicity for a membrane.

**Fig. 11.** Contact angle values Vs. the percentages of GO in the membranes

Having several oxygen-containing functional groups as carboxyl, epoxy and hydroxyl groups, GO supported the negative character of the membrane's surface leading to enhanced interaction of membrane and water molecules, resulting in increased hydrophilicity indicating that water molecules have a strong attraction for the membrane surface. Allowing for more water flow due to the growing affinity toward targeted water molecules, the improved membrane -concerning hydrophilicity- showed enhanced permeation water flux. These interactions between the several oxygen-containing functional groups in the GO plane and the exposed hydroxyl groups in CA were attributed to hydrogen bonds.

Asymmetric membranes of CA were prepared using phase inversion based on their outstanding filtration character due to their high permeation rates as well as high salt rejection values [47]. Increase in polymer concentration leads to decreasing the pore diameter which can be the pathway for improved salt rejection rates as previously proposed by Saljoughi, E. et al. [52] and Sofiah, H. et al. [53].

### 3.5 Permeation and salt rejection rates

Performance of the prepared membranes was evaluated by detecting their permeation and salt rejection rates according to equations 1 and 2. The concerned membranes were tested via Sterlitech HP4750 Stirred Cell (a dead-end cell filtration system) to investigate the permeation flow and salt rejection rates. A pressure of 10 bars was applied for an appropriate permeation flow.

A solution of NaCl with a concentration of 2000 ppm was employed as the feeding solution resembling brackish water containing a high concentration of chloride (Cl<sup>-</sup>) ions with an average concentration of 2200 ppm [16]. The feeding solution passed through an area of 14.6 cm<sup>2</sup> in the pressurized flow-through system. Both permeation rate and salt rejection % were determined according to equations 1 and 2 [17]. Concentrations of both permeate and solutions were measured by Cond 330i (WTW 82362 Welheim) device.

The casted membrane of crude CA (developed from palm fiber), was tested for its performance through the filtration process. The tested membrane was evaluated taking into consideration its permeation and salt rejection rates (**table.4**). The experiment was carried out 3 times and average values were estimated. The added GO membranes were also evaluated the same way.

Results revealed that the permeation rate for crude CA membrane was 0.009 L/m<sup>2</sup>h while its salt rejection percentage was 44 %. Along with the addition of GO to the CA membranes, improved performance was noticed for the prepared membranes. The ability to draw water molecules, is supported greatly by the hydrophilicity of membrane's bringing about enhanced rate of water permeation [15]. Loading started with 0.01 % of graphene oxide, resulting in enhanced average permeation rate as 0.013 (L/m<sup>2</sup>h.bar). Increasing the concentration of GO to 0.02 and 0.05 % led to further improved permeation rate evaluated as 0.02 and 0.026 (L/m<sup>2</sup>h.bar) respectively which can be attributed to the formation of suitable water pathways or channels through the involved pores. So, the average route was increased, which led to a reduction in the permeate flow. Further adding as much as 0.1 % caused a considered decline being estimated as 0.024 (L/m<sup>2</sup>h.bar) as illustrated in **Fig. 12**.

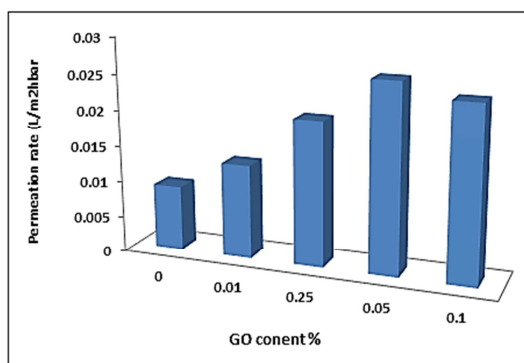


**Fig. 12.** Permeation rate values Vs. the percentages of GO in the membranes

Excessive addition of graphene oxide played a different role pertaining to the expected values of permeation rate. The experimental findings refer to the decline in permeation rate for the CA membrane loaded with 0.1 % which can be attributed to the dimensioned pore size as expected being a logic interpretation due to the successive accumulation of salts and the passage pathways getting narrower more and more.

Reduced size of pores can be promoted by delayed demixing during membrane preparation. Viscosity is the reason to blame for, ascending viscosity delay demixing and render to reduced size of pores that is on the contrary a merit for salt rejection ability.

Augmenting the membrane performance, doping with successive concentrations of GO as 0.01, 0.02, 0.05 could indeed heighten the salt rejection

rate as present in **Fig. 13** to be 49.3, 53.6, 67.5 and 69.1 % respectively due to the improved permeability and selectivity [54, 55] of the developed membrane for salts passing along with water.

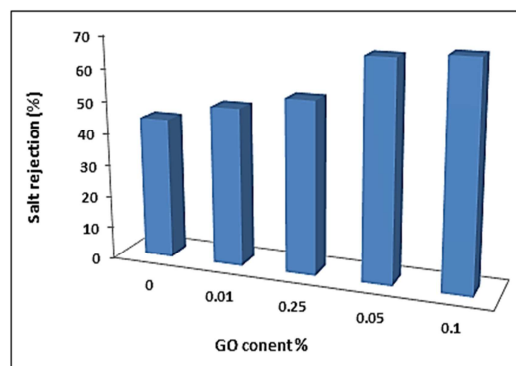


**Fig. 13.** Salt rejection % Vs. the percentages of GO in the membranes

The anti-fouling potential of CA was investigated by Hadi et al. [56] revealing that due to the hydrophilic characteristics of the membrane surface and the strong negative surface charge caused by the carboxylate groups at neutral pH, the anti-fouling behavior was seen. Through this work, the addition of graphene oxide could also contribute to the anti-fouling properties supposed to the membranes. Results included inhere refer to the enhanced hydrophilicity of all membranes with different amounts of GO. Having several oxygen-containing functional groups as carboxyl, epoxy and hydroxyl groups. The negative character of the membrane's surface was supported by GO, leading to enhanced interaction of membrane and water molecules, resulting in increased hydrophilicity. Jin et al. [57] also believed that graphene oxide (GO) could be utilised to increase membrane hydrophilicity and reduce fouling on membranes.

The prepared membranes belonging to this work can be a tool for facing the present worrying problems including the accumulation of agricultural biomass and the shortage in water resources or the unsatisfying quality of it.

#### Conflict-of-interest

The authors have no conflicts of interest to declare. All co-authors have seen and agree with the contents of the manuscript and there is no financial interest to report. We certify that the submission is original work and is not under review at any other publication.

#### Conclusion

In this study, fibers of *Phoenix dactylifer* were chemically pulped by alkali hydrolysis with NaOH to separate hemicellulose and

lignin and finally get pure cellulose that was further designed into a microcrystalline form for a much better acetylation reaction with acetic anhydride. Fractions separated and produced through the whole steps, were chemically characterized via spectroscopic method i.e IR. Date palm fibers were proved to be a promising source of cellulose from which cellulose acetate (CA) was developed and experienced as a membrane-based material. GO prepared from palm fibers was added to the developed CA in the casting solution, producing a well-defined and employed bunch of membranes involved in water treatment and salt removal with enhanced properties that that of crude CA.

#### Acknowledgment

Authors are grateful to the sincere support devoted by NRC and The Holding Company for Drinking Water in Menufia.

#### References

- [1] Sreekala M. S., George J., Kumaran M. G. and Sabu T., The mechanical performance of hybrid phenol-formaldehyde-based composites reinforced with glass and oil palm fibres, *Composites Science and Technology*, 623, 339-353 (2002).
- [2] Habibi Y., Lucia L.A. and Rojas O.J., Cellulose Nanocrystals: Chemistry, Self-Assembly, and Applications. *Chemical Reviews*, 110, 3479-3500 (2010).
- [3] Compton O.C., Cranford S.W., Putz K.W., An Z., Brinson L.C., Buehler M.J. and Nguyen, S.T., Tuning the mechanical properties of graphene oxide paper and its associated polymer nanocomposites by controlling cooperative intersheet hydrogen bonding. *ACS Nano*, 6 (3), 2008-2019 (2012).
- [4] Lee J., Chae H.-R., Won Y.J., Lee K., Lee C.-H., Lee H.H., Kim I.-C. and Lee J., Effect of graphene oxide (GO) on the surface morphology & hydrophilicity of polyethersulfone (PES). *J. Membr. Sci.* 448, 223 (2013).
- [5] Jiao Y., Song L., Zhao C., An Y., Lu W., He B. and Yang C., Membrane-based indirect power generation technologies for harvesting salinity gradient energy- A review. *Desalination*, 525, 115485 (2022).
- [6] Panagopoulos A., Haralambous K. J. and Loizidou M., Desalination brine disposal methods and treatment technologies- A review. *Science of the Total Environment*. 693: 133545 (2019).
- [7] AOAC. (1970). Official Methods of Analysis of the Association of Official Analysis Chemists. 11 th Edn., Association of Official Analytical Chemists, Washington, DC., USA.
- [8] Debois M., Gilles K.A., Hamilton J.K., Rebers P.A. and Smith F., Colorimetric method for determination of sugars and related substances. *Analytical Chemistry*, 28 (3), 350-356 (1956).
- [9] Jayme G. and Knolle, Paper chromatography of sugar mixtures on glass fiber papers. *Angew. Chemie Int. Edn.*, 68:243-246 (1956).
- [10] Partridge S.M., Aniline hydrogen phthalate as a spraying reagent for chromatography of sugars. *Nature*. 164: 443-446 (1949).
- [11] Wilson C.M., Quantitative determination of sugars on paper chromatograms. *Anal. Anal. Chem.*, 31:1199-1201(1959).
- [12] Sun R., Lawther G.M. and Banks W.B., Isolation and characterization of hemicellulose B and cellulose from pressure refined wheat straw. *Ind. Crops Prod.*, 7:121-128 (1998).
- [13] Hummers W.S. and Offeman R.E., Preparation of graphitic oxide. *Journal of the American Chemical Society*, 80, 1339-1339 (1958).
- [14] Ragab T. I. M., Amer H., Wasfy A. A. F., Abdel Hady M. S., Abdel Tawab H. and Liebner F., Sulfated cellulose from agriculture wastes, anticoagulant, fibrinolytic and toxicological studies. *J Environ Sci Technol.*, 7(5), 266-280 (2014)a.
- [15] Madina Mahmmod, Modification of cellulose acetate membranes with graphene oxide nanofillers for water treatment. Msc. Thesis, American University in Cairo, Cairo, Egypt. (2017).
- [16] Schubert H., Schories D., Schneider B. and Selig U., Brackish water as an environment. *Biological Oceanography of the Baltic Sea*, pp. 3-21 (2017). Springer Netherlands.
- [17] Kucera J., Reverse Osmosis Design, Processes, and Applications for Engineers. Co-published by John Wiley & Sons, Inc. Hoboken, New Jersey, and Scrivener Publishing LLC, Salem, Massachusetts, p. 23 (2010).
- [18] Tonghua Z., Min G., Lan C. and Xiaolong L., Investigations on the structure and properties of palm leaf sheath fiber. *Cellulose*, 22, 1039-1051 (2015).
- [19] Bourmaud A., Malvestio J., Lenoir N., Siniscalco D., Habrant A., King A., Legland D., Baleya C. and Beaugrand J., Exploring the mechanical performance and in-plant architecture of secondary hemp fibers. *Industrial Crops & Products*, 108,1-5 (2017).
- [20] Sbiai A, Maazouz A., Fleury E., Sautereau H. and Kadimi H., Short date palm tree fibers/polyepoxy composites prepared using Rtm process: effect of tempo mediated oxidation of the fibers. *Bioresources*, 5, 672-689 (2010).
- [21] Pradeep P. and Edwin R. D. J., Characterization of chemical and physical properties of palm fibers. *J. Advances in Materials Science and Engineering: An International Journal (MSEJ)*, 2, 4, 1-6 (2015).
- [22] Reneta Y., Foba-Tendo J., Njeugna E., Oliver G. and Cooke K. O., Extraction and characterization of fibers from the stalk and spikelets of empty fruit bunch (EFB). *Journal of Applied Chemistry*, 3, 1-10 (2015).
- [23] Abdul Khalil H. P. S., Nur Firdaus M. Y., Anis M. and Ridzuan R., The effect of storage time and humidity on mechanical and physical properties of medium density fiberboard (mdf) from oil palm empty fruit bunch and rubberwood.

- Polymer-Plastics Technology and Engineering*, 47, 10,1046 – 1053 (2008).
- [24] Ragab T I. M., Shalaby A. G., El Awdan S. A., Refaat A. and A. Helmy W, New applied pharmacological approach/trend on utilization of agro-industrial wastes. *Environmental Science and Pollution Research*, 25,26446–26460 (2018).
- [25] Ragab T I. M., Wasfy A. A. F., Amer H., El-Gendi A., Abdel-Hady M. S. and Leibner F., Synthesis of cellulose acetate membrane from the Egyptian rice straws. *Journal of Applied Sciences*, 14 (24), 3424-3435 (2014)b.
- [26] Kačuráková M., Belton P. S., Wilson R. H., Hirsch J. and Ebringerová A., Hydration properties of xylan-type structures: an FTIR study of xylooligosaccharides. *J Sci Food Agric.*, 77, 38–44 (1998).
- [27] Marchessault R. H. and Liang C. Y., The infrared spectra of crystalline polysaccharides. VIII. Xylans. *J PolymSci.*, 59, 367–378 (1962).
- [28] Gupta S, Madan RN and Bansal MC., Chemical composition of Pinuscaribea hemicellulose. *Tappi J.*, 70, 113-116 (1987).
- [29] Suna R.C., Tomkinson J., Wang Y.X. and Xiao B., Physico-chemical and structural characterization of hemicelluloses from wheat straw by alkaline peroxide extraction. *Polymer*, 41, 2647–2656 (2000).
- [30] Abdul Latif M. H., Attiya H. G., Al–Abayaji M. A. and Alsouz M. A. K., Isolation and characterization of lignin from Iraqi date palm *Phoenix Dactylifera*L. frond bases as a good and cheap source of lignin. *Journal of Natural Sciences*, 5, 4:83-89 (2006).
- [31] Watkins D., Nuruddin M., Hosur M., Tcherbi-Narteh A. and Jeelani S., Extraction and characterization of lignin from different biomass resources. *Journal of Materials Research and Technology*, 4, 1, 26-32 (2015).
- [32] Nabili A., Fattoum A., Passas R. and Elaloui E., Extraction and characterization of cellulose from date palm seeds (*phoenix dactylifera L.*). *Cellulose Chem. Technol.*, 50, (9-10), 1015-1023 (2016).
- [33] Mandal A., and Chakrabarty D., Isolation of nanocellulose from waste sugarcane bagasse (SCB) and its characterization. *Carbohydr. Polym.*, 86, 1291-1299 (2011).
- [34] Kumar A., Negi Y. S., Choudhary V. and Bhardwaj N. K., Characterization of cellulose nanocrystals produced by acid hydrolysis from sugarcane bagasse as agro-waste. *Journal of Materials Physics and Chemistry*, 2 (1), 1-8 (2014).
- [35] Zain N. F. M., Yusop S. M. and Ishak A. I., Preparation and characterization of cellulose and nanocellulose from pomelo (*Citrus grandis*) albedo. *Nutr Food Sci.*, 5: 1 (2014).
- [36] Hindi S. S. Z., Suitability of date palm leaflets for sulphated cellulose nanocrystals synthesis. *Nanoscience and Nanotechnology Research*, (4), 1, 7-16 (2017).
- [37] Saika, C. N., Ali F., Goswami T. and Ghosh A. C., Esterification of high  $\alpha$ -cellulose extracted from *Hibiscus cannabinus L.* *Ind. Crops Prod.*, 4:233-239 (1995).
- [38] Sun, X. F., Sun R.C. and Sun J.X., Acetylation of sugarcane bagasse using NBS as a catalyst under mild conditions for the production of oil-sorption active materials. *Bioresource. Technol.*, 95,3, 343-350 (2004).
- [39] Luz S. M., Del Tio J., Rocha G.J. M., Gonçalves A.R. and Del’Arco Jr A.P., Cellulose and cellulignin from sugarcane bagasse reinforced polypropylene composites: Effect of acetylation on mechanical and thermal properties. *Composites: Part A*, 39, 1362–1369 (2008).
- [40] Poletto, M., Ornaghi, H. L. and Zattera, A.J. Native cellulose: structure, characterization and thermal properties. *Materials*, 7, 6105–6119 (2014).
- [41] Yıldız S., Morcali M. H., Ziba C.A., Copcu B. and Dolaz M., Synthesis and characterization of cellulose derivatives from industrial towel waste. *Chemistry Select*, 4, 8358–8364 (2019).
- [42] Mustafa H. Hafez, Gehad G. Mohamed, Mohamed M. Omar, Maher M.I. El-Dessouky, Tarek S. Jamil. Preparation and Characterization of Graphene Oxide from Agriculture Waste for Water Treatment. *Egypt. J. Chem.*, 67, 3, 181- 193 (2024).
- [43] Wilkie J. S., Carl Nageli and the fine structure of living matter. *Nature*, 190,1145–1150 (1961).
- [44] Shahriary L. and Athawale A. A., Graphene oxide synthesized by using modified hummers approach. *Int. J. Renew. Energy Environ. Eng.*, 2, 58–63 (2014).
- [45] Patpen P. P., Russly B. A., Rosnita A. T. and Khalina A., Extraction and characterization of cellulose from durian rind. *Agriculture and Agricultural Science Procedia*, 2, 237– 243 (2014).
- [46] Mulder M., Basic Principles of Membrane Technology, 2nd Edition, Kluwer Academic Publishers, Dordrecht, Netherlands. (1996).
- [47] Kim D. L., Le N. L. and Nunes S. P., The effects of a co-solvent on fabrication of cellulose acetate membranes from solutions in 1-ethyl-3-methylimidazolium acetate. *Journal of Membrane Science*, 1, 540-549 (2016).
- [48] Lee W.G., Kim D.Y. and Kang S.W., Porous cellulose acetate by specific solvents with water pressure treatment for applications to separator and membranes. *Macromol. Res.*, 26(7), 630-633 (2018).
- [49] Li F.; Sun M.; Cheng Q.; Yang B., Preparation and characterization of graphene oxide/cellulose triacetate forward osmosis membranes. In Proceedings of the International Symposium on Materials Application and Engineering (SAME 2016), Chiang Mai, Thailand, 20–21August 2016; Volume 67, p. 1015.
- [50] Ghaemi N., Madaeni S. S., Alizadeh A., Rajabi H. and Daraei P., Preparation, characterization and performance of polyethersulfone/organically modified montmorillonitenanocomposite membranes in removal of pesticides. *Journal of membrane science*, 382, 135-147 (2011).
- [51] Zhu J., M. Tian, Zhang Y., Zhang H. and J. Liu, Fabrication of a novel “loose” nanofiltration membrane by facile blending with chitosan–montmorillonitenanosheets for dyes purification. *Chemical Engineering Journal*, 265, 184-193.

- 
- [52] Saljoughi E., Sadrzadeh M. and Mohammadi T., Effect of preparation variables on morphology and pure water permeation flux through asymmetric cellulose acetate membranes. *Journal of Membrane Science*, 326(2), 627-634 (2009).
- [53] Sofiah H., Nora'aini A. and Marinah M. A., The influence of polymer concentration on performance and morphology of asymmetric ultrafiltration membrane for lysozyme separation. *Journal of Applied Sciences (Faisalabad)*, 10 (24), 3325-3330 (2010).
- [54] King W.M., Cantor P.A., Schoellenback L.W., Cannon C.R., High-retention reverse osmosis desalination membranes from cellulose acetate, in: A.F. Turbak (Ed.), *Membranes from Cellulose Derivatives*, Interscience Publisher, New York, (1970).
- [55] Sudak R. G, Reverse osmosis, in: M.C. Porter (Ed.), *Handbook of Industrial Membrane Technology*, Noyes Publication, New Jersey (1990).
- [56] Hadi P., Yang M., Ma, H., Huang X., Walker H. and Hsiao B. S., Biofouling-resistant nanocellulose layer in hierarchical polymeric membranes: synthesis, characterization and performance. *Journal of Membrane Science*, 579, 162–171 (2019).
- [57] Jin L., Wang Z., Zheng S., Mi B., Polyamide-crosslinked graphene oxide membrane for forward osmosis. *Journal of Membrane Science*, 545, 11-18 (2018).